American Mineralogist, Volume 79, pages 983–990, 1994

Crystal structure of Al-rich mullite

REINHARD X. FISCHER
Institut für Geowissenschaften der Universität, D-55099 Mainz, Germany
HARTMUT SCHNEIDER, MARTIN SCHMÜCKER
Deutsche Forschungsanstalt für Luft- und Raumfahrt, Institut für Werkstoff-Forschung, D-51147 Cologne, Germany

ABSTRACT

Mullite has been synthesized in a sol-gel process yielding an alumina-rich phase with 89 mol% Al_2O_3 corresponding to $Al_{5.65}Si_{0.35}O_{9.175}$, with 0.825 O vacancies, space group *Pbam*, $a = 7.7391(6)$, $b = 7.6108(5)$, $c = 2.9180(1)$ Å, and $Z = 1$. This is the highest alumina content observed so far in the mullite solid solution series. The correlation of lattice parameters with alumina content shows a strictly linear increase of a beyond the crossover point of a and b at 78 mol% Al_2O_3. This clearly proves that the average crystal structure remains orthorhombic and does not transform to a tetragonal form. The crystal structure has been analyzed by the Rietveld method on the basis of X-ray powder diffraction data. The refinement shows that about half an Al atom per unit cell is statistically distributed on a new T** site that is linked to T_3O groups (T_2T^*O) forming the crosslinks between the chains of AlO_6 octahedra. T** has five bonds to O atoms between 1.81 and 2.42 Å. These long distances in the average crystal structure are assumed to be shorter in the local environment of T**, which could be achieved by split O positions.

INTRODUCTION

The average crystal structure of mullite has been extensively studied for many years by a number of authors because of its extraordinary role in ceramic materials (Burnham, 1964; Angel and Prewitt, 1986; Balzar and Ledbetter, 1993; for further references see Schneider et al., 1994). Mullite is one of the promising candidates for high-temperature applications because of its low thermal expansion and conductivity, its chemical and thermal stability, and its high-temperature creep behavior (e.g., Aksay et al., 1991; Schneider et al. 1994).

Mullite has been commonly described to exist in a solid solution series of composition $Al_{4+2x}Si_{2-2x}O_{10-x}$, with an observed compositional range of $0.18 \leq x \leq 0.55$ (57–74 mol% Al_2O_3). This corresponds to the known mullite end-members, $Al_{4.36}Si_{1.64}O_{9.82}$ and $Al_{5.10}Si_{0.90}O_{9.45}$, respectively. Compositions with $x = 0$ and $x = 1$ correspond to sillimanite (Burnham, 1963) and alumina, with a hypothetical mullite-type structure (Foster, 1959; Saalfeld, 1962; Perrotta and Young, 1974; Duvigneaud, 1974; Cameron, 1977a). Mullite compositions with x near 0.25 and 0.4 have frequently been described and are designated as 3:2-mullite ($3Al_2O_3 \cdot 2SiO_2$) and 2:1-mullite ($2Al_2O_3 \cdot 1SiO_2$), respectively.

Mullite crystallizes in the orthorhombic space group *Pbam*. Cameron (1977a, 1977b), Schneider (1986), Klug et al. (1990), and Ban and Okada (1992) have shown that the chemical composition of mullite can be derived from a linear relationship between a and the alumina content. Whereas a increases upon increasing alumina content, b decreases, thus yielding a crossover point at about 78 mol% Al_2O_3 by extrapolation of the two curves (Cameron, 1977a). When $a = b$, this compound is often designated as tetragonal or pseudotetragonal mullite, but, actually, it remains orthorhombic with a symmetrically independent coincidence of a and b. However, the question remains whether mullite with a composition beyond the crossover point exists.

Recently Schneider et al. (1993) synthesized alumina-rich mullite with $a > b$, even though normal mullite is characterized by $a < b$. Our goal was to synthesize mullite with similar lattice parameters but better crystallinity that was suitable for a Rietveld analysis of its crystal structure.

EXPERIMENTAL METHODS

Sample preparation

Aluminum sec-butylate [$Al(O^iBu)_3$] and silicon tetrachloride corresponding to an Al-Si ratio of 4:1 were used as starting materials. After homogenization of the phase admixture, H_2O was added, leading to a vigorous reaction that produced a highly viscous white gel. After precalcination at 350 °C, the powder was annealed at 1000 °C for 15 h, resulting in a mullite-like compound, γ alumina, and a residual noncrystalline phase. Details of the synthesis procedure are given by Schneider et al. (1993).

Analytical transmission electron microscopy (ATEM)

Transmission electron microscopy (TEM) and microanalyses were performed with a Philips EM 430

0003–004X/94/0910–0983$02.00

TABLE 1. Experimental conditions, crystallographic data, and definitions used in data refinement

Radiation type, source	X-ray, Cu$K\alpha$
Instrumental settings	40 kV, 30 mA
Discriminator	diffracted beam, curved graphite monochromator
Detector	scintillation counter
Divergence slit	ADS
Receiving slit	0.2 mm
Data collection temperature	room temperature
Particle size	<200 nm
2θ range used in refinement	15–120°
Step size	0.04°
Counting time per step	30 s
Space group	*Pbam*
Z	1
Lattice parameters (Å) a	7.7391(6)
b	7.6108(5)
c	2.9180(1)
R_{wp} (%)	6.75
R'_p (%)	16.33
R_e (%)	3.85
R_B (%)	7.28

Definitions

$$R_{wp} = \sqrt{\frac{\Sigma_i w_i(y_{io} - C \cdot y_{ic})^2}{\Sigma w_i y_{io}^2}}$$

$$R'_p = \frac{\Sigma_i |y_{io} - C \cdot y_{ic}|}{\Sigma_i |y_{io} - y_{ib}|}$$

$$R_B = \frac{\Sigma_k |I_{ko} - C \cdot I_{kc}|}{\Sigma_k I_{ko}}$$

$$R_e = \sqrt{\frac{N - P}{\Sigma_i w_i y_{io}^2}}$$

R_{wp} = weighted residual including profile intensities
R'_p = unweighted and background-corrected residual
R_e = statistically expected residual
R_B = residual including integrated intensities
N = no. of statistically independent observations
P = no. of variable least-squares parameters
y_o, y_c = observed and calculated profile intensities
I_o, I_c = observed and calculated integrated intensities
C = scale factor
w = weight = $1/y_o$

Note: standard deviations for lattice parameters are given in parentheses.

analytical microscope (300 kV accelerating voltage, LaB_6 filament) equipped with a Tracor system for energy-dispersive X-ray spectroscopy. TEM sample preparation was performed by depositing the suspended powders on a C film.

Rietveld refinement procedures

Data were collected on a Seifert automated powder diffractometer with graphite-monochromatized Cu$K\alpha$ radiation and a zero-background quartz sample holder. Details of data collection, crystallographic data, and definitions are given in Table 1. The background was subtracted by hand, since its shape was irregular due to the coexisting glass phase and could not be fitted by a simple function. The background values were determined by linear interpolation between consecutive breakpoints in the pattern. Regions belonging to γ alumina were excluded from the refinement. Intensities within eight times the full width at half maximum of a peak were considered to contribute to the central reflection. Peaks below 50° 2θ were corrected for asymmetry effects after Rietveld (1969). Calculated intensities were corrected for automatic divergence slit effects in the Rietveld procedure. The pseudo-Voigt function was used for the simulation of the peak shape, with a refinable parameter defining the Lorentzian and Gaussian character of the peaks as a function of 2θ. Initial coordinates for the refinement in space group *Pbam* were taken from Angel and Prewitt (1986), omitting the O atom Oc, which should be completely vacant for this composition.

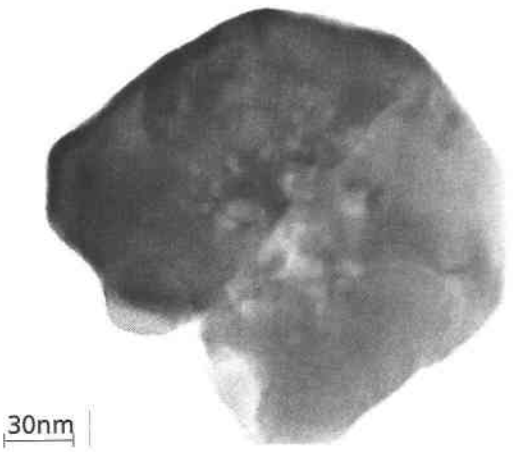

Fig. 1. A high-resolution electron microscope (HREM) photograph of a mullite crystallite.

Occupancies were set assuming fully occupied Al and O sites in the AlO_6 octahedron: 2.67 atoms (Al + Si) on the T site (2.31 Al + 0.35 Si), 1.33 Al atoms on the T* site, and, correspondingly, 1.33 O atoms on Oc*. That leaves 0.11 Al atoms not accounted for, according to the chemical analysis. This assignment is based on the assumption that not more than three $(Al,Si)O_4$ tetrahedra are linked together.

The structure analysis was performed with the PC-Rietveld plus package (Fischer et al., 1993), with a kernel program based on the Rietveld (1969) method written by Wiles and Young (1981) and extensively modified by Hill and Howard (1986). X-ray scattering factors in their respective valence states were taken from the *International Tables for X-ray Crystallography* (Ibers and Hamilton, 1974) and the values for O^{2-} from Hovestreydt (1983). The crystal structure drawings were made with the plotting program Struplo (Fischer et al., 1991), and the contour map of the difference-Fourier calculation was drawn with a new program module (M. Auernhammer, unpublished program) in the PC-Rietveld plus package.

RESULTS

Chemical composition

Because the lattice parameters of mullite are directly related to its chemical composition, the correct determination of the Al_2O_3 content is crucial. Therefore, great

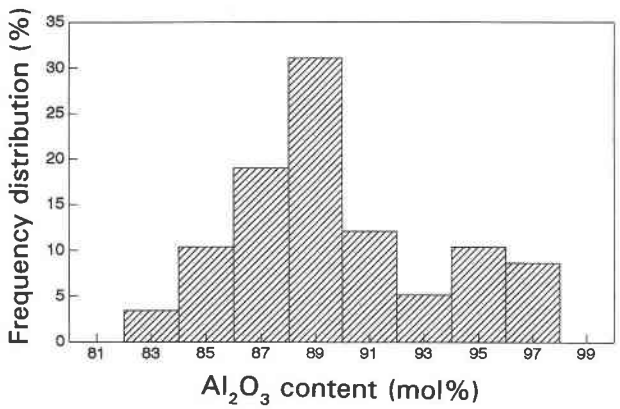

Fig. 2. The Al_2O_3 frequency-distribution range of the mullite studied here. Results are from analytical transmission electron microscope (ATEM) analyses of 58 crystallites.

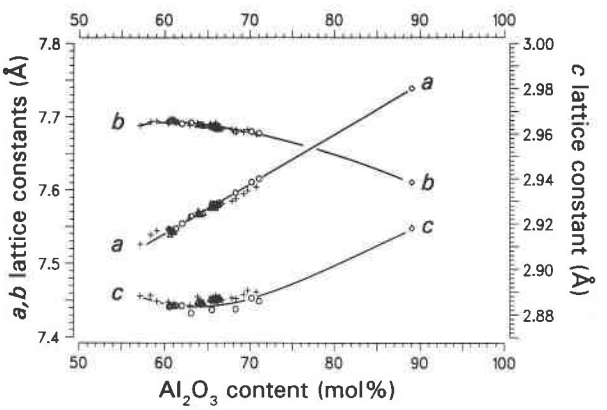

Fig. 3. The relationship between lattice parameters of mullite and Al content. Data are taken from Cameron (1977b) (crosses), Klug et al. (1990) (triangles), and Ban and Okada (1992) (open circles). The diamond-shaped symbols at 89 mol% Al_2O_3 represent results from this work. The line is hand-fitted, with the higher weight on the more recent data.

care has been taken to analyze the mullite crystallites. The analysis is made even more difficult because the mullite crystals, often embedded in an amorphous matrix, are smaller than 200 nm (Fig. 1). To get reasonable statistics, 58 analyses were performed on a large number of crystallites using ATEM. The results of these analyses are summarized in Figure 2. The Al content of the specimen studied here extends the cell parameter data beyond the crossover point of a and b at $\approx$78 mol% Al_2O_3 (Fig. 3).

The ATEM analyses show that the mullite components in the sample exhibit a relatively wide range between 83 and 97 mol% Al_2O_3, with an asymmetric distribution around the maximum of 89 mol% Al_2O_3. Such a variable composition would influence the lattice parameters, yielding ranges of about $\pm$0.04 Å for a, $\pm$0.03 Å for b, and $\pm$0.01 Å for c. Consequently, powder diffraction peaks would be broadened at their left and right tails. The maximum separation of peak positions caused by this multiphase effect, though, still would lie beyond the instrumental resolution, thus not showing any splitting of reflections. However, some weak shoulders observed at the left and right slopes of some higher-angle reflections might support this interpretation of the results of the chemical analyses. Actually, a retrospective structure refinement using the results of the single-phase refinement but simulating a three-phase diagram weighted by the amount of components with 85, 89, and 95 mol% Al_2O_3, respectively, improved the fit between observed and calculated data as expressed by a decrease of the residuals of ΔR_{wp} = 0.7%, from 6.8 to 6.1%.

Using 89 mol% Al_2O_3 as the average value for the mullite phase, we get the composition $Al_{5.65}Si_{0.35}O_{9.175}$, which is in agreement with the general formula of the solid solution series corresponding to $x = 0.825$.

Figure 3 shows the relationship between lattice parameters and Al content (after Cameron, 1977b; Klug et al., 1990; and Ban and Okada, 1992), extended for the new data point at 89 mol% Al_2O_3 represented by the mullite studied here. This shows that the curve for the lattice parameters can be extrapolated beyond the crossover point, permitting chemical compositions for the alumina-rich mullite to be estimated on the basis of its observed cell parameters.

Rietveld refinements

To obtain a starting model for the crystal structure refinement, the general mechanism of Si-Al substitution in the solid solution series must be known. Provided that there is only one substitution of one Si atom by one Al atom, and that the octahedral coordination of the AlO_6 polyhedron remains constant, the following scheme (shown in Table 2) was developed: The chemical composition given in Table 2 is split into the compositionally invariable chain of octahedra and the variable residue. The number of cations in the T_2O, T_3O, and T_4O groups are given, as well as the total number of these groups in the unit cell, which is equivalent to the coordination number of the bridging O atom. In this model, eight O atoms per unit cell are assigned to the two $^{[6]}Al$ atoms. Note that in each AlO_6 octahedron there are four O atoms that share common edges with two adjacent octahedra, thus giving the overall composition of AlO_4 (or Al_2O_8 per unit cell) for the chains of octahedra. Tetrahedrally coordinated atoms are linked to three O atoms of the octahedral chain. The tetrahedron is completed by the remaining O atoms not incorporated into the octahedra. The coordination number of this O atom (i.e., the number of tetrahedra that have this O atom as a common corner) depends on the number of the remaining O atoms. According to data in Table 2, there are four tetrahedrally coordinated atoms (T atoms) and two O atoms not incorporated into the octahedra in sillimanite. Therefore, exactly two T atoms must be linked with one bridging O atom. We designate T_2O, T_3O, and T_4O to refer to

TABLE 2. Chemical compositions and site assignments for some specific mullite samples in the solid solution series between sillimanite and ι-Al_2O_3

Compound	x	Oct. chain	Residue	No. of T,T* sites			No. of groups		
				T_2O	T_3O	T_4O	T_2O	T_3O	T_4O
Sillimanite	0	Al_2O_8	$Al_2Si_2O_2$	4	0	0	2	0	0
3:2-mullite	0.25	Al_2O_8	$Al_{2.5}Si_{1.5}O_{1.75}$	2.5	1.5	0	1.25	0.5	0
2:1-mullite	0.4	Al_2O_8	$Al_{2.8}Si_{1.2}O_{1.6}$	1.6	2.4	0	0.8	0.8	0
4:1-mullite	⅔	Al_2O_8	$Al_{3.33}Si_{0.67}O_{1.33}$	0	4	0	0	1.33	0
89% mullite	0.825	Al_2O_8	$Al_{3.65}Si_{0.35}O_{1.175}$	0	2.1	1.9	0	0.7	0.475
ι-Al_2O_3	1	Al_2O_8	Al_4O	0	0	4	0	0	1

Note: x number of O vacancies. T_3O and T_4O groups are composed of T_2T^*O and $T_2T^*T^{**}O$ units, respectively.

configurations where one O atom (Oc in T_2O, Oc* in T_3O and T_4O) bridges two, three, and four T atoms, respectively. In the 3:2-mullite, four T atoms share 1.75 O atoms, which gives a configuration with 1.5 T atoms in T_3O groups and 2.5 T atoms in T_2O groups. Consequently, 1.25 O atoms are linked to two T atoms, and 0.5 O atoms to three T atoms. In 2:1-mullite, there is an equal number of T_3O and T_2O groups, and the 4:1-mullite consists of T_3O groups only. A hypothetically ordered structure of this type corresponding to a $3 \times a$ orthorhombic supercell is shown in Figure 4. The transformed coordinates, together with the transformation matrices, are given in Table 3. This model represents one possibility for a local arrangement of the unit cells in mullite. A statistical distribution of the T_3O groups and O vacancies gives the average structure. A further increase of the Al content, as observed in the present work, implies that new configurations for the additional Al atoms must be found. On the basis of this assumption, three models are proposed:

1. Placing the Al atoms on vacant T* sites into the B voids, which converts some of the existing T_3O groups (Fig. 4) into T_4O groups.
2. Placing Al into the B voids (Fig. 4) but off the T* site in the environment of the O atom bridging the tetrahedra.
3. Placing Al on an interstitial site in the big elliptical A voids (Fig. 4), with contacts to the chains of octahedra only.

In any case, the framework structure consisting of the 4:1-mullite shown in Figure 4 will be the main constituent of the crystal structure of the 8:1-mullite studied here. The difference occurs in the T site, which has a different Al-Si ratio. Therefore, the following assumptions were made for the initial refinement: fully occupied octahedral sites (Al and Oab, Od), 2Al and 0.35Si in the T position, 1.175Al in T*, and 1.175O in Oc*. Si and Al are distributed over the T and T* sites, with the assumption of a 2:1 ratio between the number of T and T* atoms and assigning all Si to the T position.

On the basis of this model, the Rietveld refinement yielded residuals of $R_{wp} = 7.0\%$ and $R_B = 8.5\%$, thus confirming that the crystal-structure model is essentially correct. However, a negative displacement factor for T* indicated a deficiency in its population. Subsequent difference-Fourier analysis showed a distinct maximum at 0.35, 0.12, 0.5 with 8 e/Å^3 (Fig. 5). This position is close to the T* site and thus would conform with model 1 and model 2, but it disagrees with model 3. Fourier results are generally less significant in a powder-diffraction case than they are in the single-crystal case because of pattern-deconvolution problems. However, this position is the only characteristic feature in the Fourier maps that repeatedly and reproducibly occurs in the Fourier calculations after various refinements. Therefore, refinements were performed that allowed a comparison of model 1 and 2 assignments.

Model 1. The remaining Al atoms reside in the T* position, building additional links to the bridging O atom in the T_3O groups, thus forming T_4O groups (Fig. 6). It is evident from Figure 4 that the additional T* atom should cause a shift of the O atom toward the center of the cross built by the two T atoms and the two T* atoms. This actually is the Oc position at 0.5,0,0.5. If the link between opposite T* atoms would be through Oc*, a tug of war for the bridging O atom toward one of the T*

TABLE 3. Coordinates transformed to $3 \times a$ supercell in *Pbam* representing a hypothetically ordered supercell of 4:1-mullite

Atom	x	y	z	Matrix no.†	Wyckoff pos.	Site sym.	No. of atoms per unit cell
Al1	⅙	0	0	1	4*g*	..*m*	4
Al2	½	0	0	2	2*c*	..2/*m*	2
T1	0.2160	0.3317	½	1	4*h*	..*m*	3Al/1Si
T2	0.1174	0.6683	½	3	4*h*	..*m*	3Al/1Si
T*	0.5863	0.2203	½	2	4*h*	..*m*	4Al
Od1	0.2112	0.2164	0	1	4*g*	..*m*	4
Od2	0.5445	0.2164	0	2	4*g*	..*m*	4
Od3	0.8779	0.2164	0	4	4*g*	..*m*	4
Oab1	0.1180	0.0791	½	5	4*h*	..*m*	4
Oab2	0.4513	0.0791	½	6	4*h*	..*m*	4
Oab3	0.7847	0.0791	½	7	4*h*	..*m*	4
Oc*	0.1567	0.4720	½	5	4*h*	..*m*	4

Note: Wyckoff position and site symmetry from *International Tables of Crystallography* (Hahn, 1983).

† Augmented matrices corresponding to transformations of the coordinates in Table 4:

$$1.\begin{pmatrix} ⅓ & 0 & 0 & ⅙ \\ 0 & 1 & 0 & 0 \\ 0 & 0 & 1 & 0 \\ 0 & 0 & 0 & 1 \end{pmatrix} \quad 2.\begin{pmatrix} ⅓ & 0 & 0 & ½ \\ 0 & 1 & 0 & 0 \\ 0 & 0 & 1 & 0 \\ 0 & 0 & 0 & 1 \end{pmatrix} \quad 3.\begin{pmatrix} -⅓ & 0 & 0 & ⅙ \\ 0 & -1 & 0 & 1 \\ 0 & 0 & 1 & 0 \\ 0 & 0 & 0 & 1 \end{pmatrix} \quad 4.\begin{pmatrix} ⅓ & 0 & 0 & ⅚ \\ 0 & 1 & 0 & 0 \\ 0 & 0 & 1 & 0 \\ 0 & 0 & 0 & 1 \end{pmatrix}$$

$$5.\begin{pmatrix} ⅓ & 0 & 0 & 0 \\ 0 & -1 & 0 & ½ \\ 0 & 0 & 1 & 0 \\ 0 & 0 & 0 & 1 \end{pmatrix} \quad 6.\begin{pmatrix} ⅓ & 0 & 0 & ⅓ \\ 0 & -1 & 0 & ½ \\ 0 & 0 & 1 & 0 \\ 0 & 0 & 0 & 1 \end{pmatrix} \quad 7.\begin{pmatrix} ⅓ & 0 & 0 & ⅔ \\ 0 & -1 & 0 & ½ \\ 0 & 0 & 1 & 0 \\ 0 & 0 & 0 & 1 \end{pmatrix}.$$

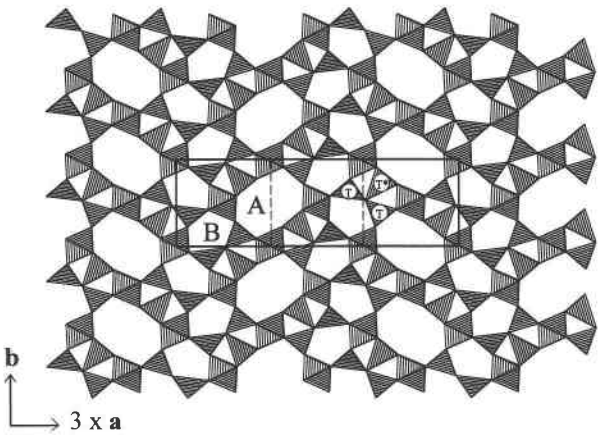

Fig. 4. The hypothetically ordered crystal structure of 4:1 mullite corresponding to a 3 × *a* orthorhombic supercell. The subcell of the average structure is marked by dashed lines. Two types of cavity in mullite are labeled A and B, respectively. Atom sites T and T* are marked in one T_3O group (T_2T^*O). Transformed coordinates and transformation matrices are given in Table 3.

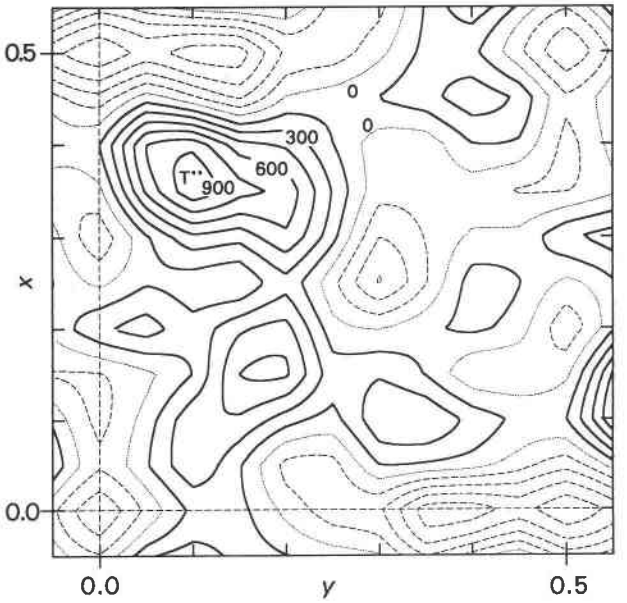

Fig. 5. A contour plot (at $z = 0.5$) of the difference-Fourier calculation. The dashed lines represent the zero level. The solid lines are drawn in equidistant steps of 150 units on the basis of the electron density scaled to 999 (corresponding to 8 e/Å³) for the highest peak.

atoms would result in T*-O distances much longer than 2.5 Å, which is very unlikely to occur in tetrahedral coordination. There would be no reason for the bridging O atom to avoid the most favorable position in the center of the four cations. Therefore, the structure model is modified by shifting 0.475 Oc* atoms to the Oc position.

The refinement based on this configuration yielded residuals of $R_{wp} = 7.1\%$ and $R_B = 8.7\%$, which is slightly worse than for the model with the 4:1-mullite structure. In addition, the unfavorable distance of 2.49 Å for T*-Oc bonds and the negative displacement factors for T (−0.14 Å²) and Oc* (−1.8 Å²) discredit this model.

Model 2. In this model, the additional Al atoms were placed exactly on the values corresponding to the maximum in the difference-Fourier analysis. The position was constrained to lie at *x,y*,0.5, and the displacement factor was fixed at 3 Å², taking into account that the position might be slightly off the mirror plane, as indicated by interpolation of the Fourier maxima around $z = 0.5$. The residuals decreased to $R_{wp} = 6.8\%$ and $R_B = 7.3\%$. Especially the decrease in R_B, which is the best measure for the crystal structure fit, from 8.5 to 7.3%, indicates that the route followed in model 2 may be on the right track. All displacement factors are positive, and the interatomic distances become more plausible. Therefore, this model is favored in the following discussion. A projection of the atom positions is shown in Figure 7.

The fit between observed and calculated diffraction patterns is shown in Figure 8. The refined atomic parameters are listed in Table 4, and a selection of interatomic distances is given in Table 5.

Discussion

The Al-Si substitution and the concomitant increase of O vacancies alone are not sufficient to describe the relationships in Al-rich mullite with $x > 0.67$. It has been postulated that additional Al has to be incorporated interstitially. The general considerations discussed above showed already that additional interstitial Al atoms should be connected with the bridging Oc* atom in the T_3O groups. Formally, the easiest solution to accommodate the additional Al atoms would be in T_4O groups. This

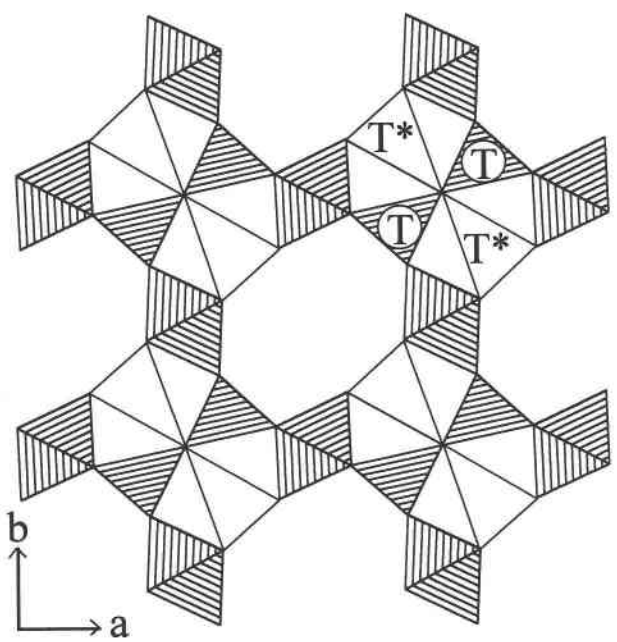

Fig. 6. A projection of a hypothetical crystal structure with T_4O groups ($T_2T^*_2O$).

TABLE 4. Positional parameters, isotropic displacement factors (Å²), site symmetry, Wyckoff positions, and occupancies

Atom	x	y	z	B	Site symm.	Wyckoff pos.	No. of atoms per unit cell
Al	0	0	0	1.93(8)	..2/m	2a	2
T	0.1479(5)	0.3317(4)	½	0.16(6)	..m	4h	2Al/0.35Si
T*	0.259(1)	0.2203(9)	½	0.5(1)	..m	4h	1.175Al
T**	0.335(3)	0.103(3)	½	3	..m	4h	0.475Al
Oab	0.3539(6)	0.4209(5)	½	1.9(1)	..m	4h	4
Oc*	0.470(3)	0.028(3)	½	4.2(5)	..m	4h	1.175
Od	0.1336(7)	0.2164(5)	0	2.9(1)	..m	4g	4

Note: data for site symmetry and Wyckoff position taken from *International Tables of Crystallography* (Hahn, 1983).

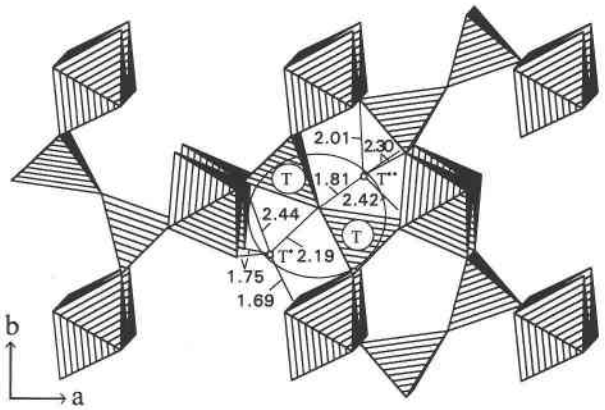

Fig. 7. A projection of the crystal structure of the mullite studied here, with T* and T** positions marked in adjacent B voids. The T_4O group ($T_2T^*T^{**}O$) is encircled.

model would permit the extension of the solid solution series to a pure ι-Al_2O_3 structure. The projection of a hypothetical structure of this type is shown in Figure 6. However, a mullite-type structure with T_4O clusters has been clearly discredited by Padlewski et al. (1992) on the basis of energy calculations. Also, the results of our study show that a symmetrical T_4O configuration is very unlikely to occur.

However, the results achieved in this study still favor a model where the bridging O atom is connected to four cations. In contrast to model 1, the additional Al atom occupies a position approximately in the center of void B in Figure 4. The Al atom is coordinated with five O atoms between 1.8 and 2.4 Å, with a mean value of 2.17 Å. Also the T* position could be better described by a fivefold coordination rather than tetrahedral coordination. Therefore, we could infer from these results that mullite with a composition beyond 80% Al_2O_3 generally consists of sillimanite-like T_2O groups, with additional pairs of Al atoms that are linked to the bridging O atom being loosely bound with long distances to the octahedral chains. This would explain that the TO_4 tetrahedra in this refinement are geometrically more regular than normally observed in mullite and that the T* sites are more distorted than usually observed. The individual T-O distances determined by Angel and Prewitt (1986) and Angel et al. (1991) for the average structure of 2:1-mullite range from 1.67 to 1.73 Å, whereas the corresponding range in the Al-rich mullite studied here is 1.71–1.74 Å. The distortion of the configuration around the T* atom is expressed by the distances ranging from 1.69 to 2.19 Å (2.44 Å in fivefold coordination) as compared with the distances between 1.77 and 1.86 Å in the 2:1-mullite.

The T**-O distances determined here are considerably longer than expected for Al-rich cation sites. However, in the discussion of interatomic distances, we should note that the refinement of T** with <½ Al atom per unit cell yields a statistical atom distribution in the average structure of mullite. Therefore, the local environment of the atoms close to the T** site may deviate slightly from the average structure. If split positions for O atoms would be considered, as proposed by Angel et al. (1991) for 2:1-mullite, we could get significantly smaller distances in the coordination polyhedron of the T** atom. Splitting Oab and Od, giving additional positions at 0.351,0.365,0.5, and 0.160,0.202,0.935, would yield distances of 2 Å between T** and Oab and Od, respectively. However, single-crystal data with intensities better resolved than in the powder-diffraction case would be required to prove such a configuration.

The formal calculation of distances yields a value of 1.19 Å between T** and Oc*. Because of the partial occupation of both sites, this distance does not occur in the local environment of T** within the unit cell. It represents the projection of all unit cells averaged in the X-ray diffraction analysis.

TABLE 5. Selected interatomic distances (Å)

4 × Al-Oab	1.942(3)	2 × T-Od	1.706(3)	T*-Oab	1.694(8)	T**-Oc*	1.81(3)
2 × Al-Od	1.945(4)	T-Oab	1.733(6)	2 × T*-Od	1.753(5)	T**-Oab	2.01(2)
		T-Oc*	1.74(3)	T*-Oc*	2.19(3)	T**-Oab	2.42(20
		[T-Oc*	1.75(3)]	T*-Oab	2.440(8)	2 × T**-Od	2.30(2)
Mean	1.943		1.72		1.97 [V]		2.17
					1.85 [IV]		
Ban and Okada (1992)	1.912		1.71		1.79		—
Angel and Prewitt (1986)	1.908		1.71		1.80		—

Note: values in brackets for T-Oc* denote the alternate coordination statistically possible in the average structure. Mean values for T*-O distances are given for fourfold-coordinated [IV] and for fivefold-coordinated [V] T* atoms.

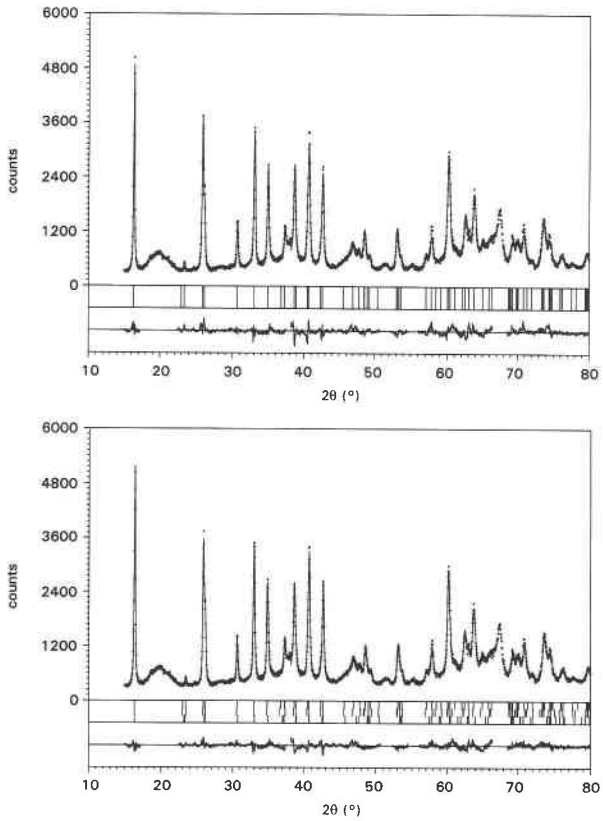

Fig. 8. Observed (crosses) and calculated (solid line) powder patterns with difference curves underneath. Peak positions permitted by the cell metric are indicated by tick marks. (**top**) Single-phase diagram. (**bottom**) Diagram resulting from a multiphase refinement based on lattice parameters inferred from ATEM analyses (Fig. 2), weighed according to the number of crystallites with 85, 89, and 95 mol% Al_2O_3, respectively.

As a general scheme, we can now summarize the following relationships between O vacancies, occupancies, distribution of T_2O, T_3O, and T_4O, and alumina content using the generally accepted substitution scheme, finally confirmed by Angel and Prewitt (1986) combined with the results from this work: The general unit-cell composition in the solid solution series is $Al_{4+2x}Si_{2-2x}O_{10-x}$, with x representing the number of O vacancies per unit cell, theoretically ranging from 0 (sillimanite) to 1 (ι-Al_2O_3). The highest value observed so far is $x = 0.825$ for the mullite studied here, not considering the Al_2O_3 phases that are described as having a mullite-type structure but without support from a structure determination. Site occupation assignments are given in Table 6. At $x = 2/3$, all Oc atoms are vacant or they are shifted to the Oc* position where they are coordinated by two T atoms and one T* atom. Toward higher alumina content, the T** sites are formed building the T_4O groups.

The assignments in Table 6 are based on the assumption that all Si atoms are incorporated in the T site. Angel and Prewitt (1986) and recently Balzar and Ledbetter (1993) did observe in occupancy refinements of the tetrahedral sites that small amounts of Si reside on T* as well. However, as pointed out by Angel and Prewitt (1986), these assignments are very uncertain, and the results are not conclusive. An occupancy of 0.033 for Si on the T* site, corresponding to 0.1 Si atoms per unit cell, was determined by Balzar and Ledbetter (1993) in the 3:2-mullite. It is very difficult to verify the incorporation of such small amounts of Si in the tetrahedral sites by Rietveld analyses. However, the Al and Si distribution on the T sites and T* sites could be reconsidered when more precise data from single-crystal analyses are available.

Table 6. Site occupancies and atom distribution as function of number x of O vacancies

	$x \leq 2/3$	$x \geq 2/3$
No. of T atoms (Si + Al)	$4 - 2x$	$4 - 2x$
No. of T* atoms (all Al)	$2x$	$2 - x$
No. of T** atoms (all Al)	0	$-2 + 3x$
No. of Al in T site	2	2
No. of Si in T site	$2 - 2x$	$2 - 2x$
No. of Oc atoms	$2 - 3x$	0
No. of Oc* atoms	$2x$	$2 - x$

Note: positions not listed are fully occupied.

Acknowledgments

We thank the Deutsche Forschungsgemeinschaft for financial support under grant Fi442/1. The award of a Heisenberg fellowship to R.X.F. is gratefully acknowledged. We would like to thank W.H. Baur and M. Gunter for their reviews of the manuscript. Computing facilities were financially supported by the Materialwissenschaftliches Forschungszentrum of the University of Mainz.

References cited

Aksay, I.A., Dabbs, D.M., and Sarikaya, M. (1991) Mullite for structural, electronic, and optical applications. Journal of the American Ceramic Society, 74, 2343–2358.

Angel, R.J., and Prewitt, C.T. (1986) Crystal structure of mullite: A reexamination of the average structure. American Mineralogist, 71, 1476–1482.

Angel, R.J., McMullan, R.K., and Prewitt, C.T. (1991) Substructure and superstructure of mullite by neutron diffraction. American Mineralogist, 76, 332–342.

Balzar, D., and Ledbetter, H. (1993) Crystal structure and compressibility of 3:2 mullite. American Mineralogist, 78, 1192–1196.

Ban, T., and Okada, K. (1992) Structure refinement of mullite by the Rietveld method and a new method for estimation of chemical composition. Journal of the American Ceramic Society, 75, 227–230.

Burnham, C.W. (1963) The crystal structure of mullite. Carnegie Institution of Washington Year Book, 62, 158–165.

——— (1964) Crystal structure of mullite. Carnegie Institution of Washington Year Book, 63, 223–227.

Cameron, W.E. (1977a) Mullite: A substituted alumina. American Mineralogist, 62, 747–755.

——— (1977b) Composition and cell dimensions of mullite. Ceramic Bulletin, 56, 1003–1007, 1011.

Duvigneaud, P.H. (1974) Existence of mullite without silica. Journal of the American Ceramic Society, 57, 224.

Fischer, R.X., Le Lirzin, A., Kassner, D., and Rüdinger, B. (1991) STRUPLO'90, eine neue Version des Fortran Plotprogramms zur Darstellung von Kristallstrukturen. Zeitschrift für Kristallographie, suppl. issue no. 3, 75.

Fischer, R.X., Lengauer, C., Tillmanns, E., Ensink, R.J., Reiss, C.A., and Fantner, E.J. (1993) PC-Rietveld plus, a comprehensive Rietveld analysis package for PC. Materials Science Forum, 133–136, 287–292.

Foster, P.A. (1959) The nature of alumina in quenched cryolite-alumina melts. Journal of the Electrochemical Society, 106, 971–975.

Hahn, T., Ed. (1983) International tables for crystallography, vol A, p. 272–273. Kluwer, Dordrecht, The Netherlands.

Hill, R.J., and Howard, C.J. (1986) A computer program for Rietveld analysis of fixed wavelength X-ray and neutron powder diffraction patterns. Report no. AAEC/M112. Australian Atomic Energy Commission (now ANSTO) Research Establishment, Lucas Heights, N.S.W., Australia.

Hovestreydt, E. (1983) On the atomic scattering factor for O^{2-}. Acta Crystallographica, A39, 268–269.

Ibers, J.A., and Hamilton, W.C., Eds. (1974) International tables for X-ray crystallography, vol. 4, p. 99–149. Kynoch, Birmingham, U.K.

Klug, F.J., Prochazka, S., and Doremus, R.H. (1990) Alumina-silica phase diagram in the mullite region. Ceramic Transactions, 6, 15–43.

Padlewski, S., Heine, V., and Price, G.D. (1992) Atomic ordering around the oxygen vacancies in sillimanite: A model for the mullite structure. Physics and Chemistry of Minerals, 18, 373–378.

Perrotta, A.J., and Young, J.E. (1974) Silica-free phases with mullite-type structures. Journal of the American Ceramic Society, 57, 405–407.

Rietveld, H.M. (1969) A profile refinement method for nuclear and magnetic structures. Journal of Applied Crystallography, 2, 65–71.

Saalfeld, H. (1962) A modification of Al_2O_3 with sillimanite structure. In Transactions of the VIIIth International Ceramic Congress, p. 71–74. The Organizing Committee of the VIIIth International Ceramic Congress, Copenhagen.

Schneider, H. (1986) Formation, properties and high-temperature behaviour of mullite: Habilitationsschrift, 148 p. Faculty of Chemistry, University of Munster, Germany.

Schneider, H., Okada, K., and Pask, J.A. (1994) Mullite and mullite ceramics. Wiley, Chichester, U.K.

Schneider, H., Fischer, R.X., and Voll, D. (1993) Mullite with lattice constants $a > b$. Journal of the American Ceramic Society, 76, 1879–1881.

Wiles, D.B., and Young, R.A. (1981) A new computer program for Rietveld analysis of X-ray powder diffraction patterns. Journal of Applied Crystallography, 14, 149–151.

Manuscript received December 21, 1993
Manuscript accepted April 28, 1994